A Comprehensive Stress Test of Truncated Hilbert Space Bases against Green's function Monte Carlo in U(1) Lattice Gauge Theory

Timo Jakobs, ^{1,2} Marco Garofalo, ^{1,2} Tobias Hartung, ^{3,4} Karl Jansen, ^{5,6} Paul Ludwig, ^{1,2} Johann Ostmeyer, ^{1,2} Simone Romiti, ⁷ and Carsten Urbach ^{1,2}

¹Helmholtz-Institut für Strahlen- und Kernphysik, University of Bonn, Nussallee 14-16, 53115 Bonn, Germany

²Bethe Center for Theoretical Physics, University of Bonn, Nussallee 12, 53115 Bonn, Germany

³Northeastern University - London, Devon House, St Katharine Docks, London, E1W 1LP, United Kingdom

⁴Khoury College of Computer Sciences, Northeastern University, #202, West Village Residence Complex H, 440 Huntington Ave, Boston, MA 02115, USA

> ⁵Computation-Based Science and Technology Research Center, The Cyprus Institute, 20 Kavafi Street, 2121 Nicosia, Cyprus

⁶Deutsches Elektronen-Synchrotron DESY, Platanenallee 6, 15738 Zeuthen, Germany

⁷Institute for Theoretical Physics, Albert Einstein Center for Fundamental Physics, University of Bern, CH-3012 Bern, Switzerland (Dated: November 3, 2025)

A representation of Lattice Gauge Theories (LGT) suitable for simulations with tensor network state methods or with quantum computers requires a truncation of the Hilbert space to a finite dimensional approximation. In particular for U(1) LGTs, several such truncation schemes are known, which we compare with each other using tensor network states. We show that a functional basis obtained from single plaquette Hamiltonians – which we call plaquette state basis – outperforms the other schemes in two spatial dimensions for plaquette, ground state energy and mass gap, as it is delivering accurate results for a wide range of coupling strengths with a minimal number of basis states. We also show that this functional basis can be efficiently used in three spatial dimensions. Green's function Monte Carlo appears to be a highly useful tool to verify tensor network states results, which deserves further investigation in the future.

I. INTRODUCTION

Hamiltonian formulations of lattice gauge theories (LGTs) offer promising avenues to address previously intractable challenges, such as real-time evolution and finite density simulations in strongly coupled quantum chromodynamics. The rapid advancements in quantum computing (QC) hardware [1] and tensor network (TN) algorithms [2] indicate that these goals may soon be achievable.

A priori, the standard Kogut-Susskind Hamiltonian [3] acts on an infinite dimensional Hilbert space. More specifically, each individual gauge link is already infinite dimensional. Physical quantum hardware as well as tensor networks require a projection of this space onto finite available resources. Thus, in order to investigate lattice gauge theories in the Hamiltonian formalism, the Hilbert space of a gauge link needs to be digitised. In other words, a discrete basis needs to be devised such that its truncation efficiently approximates the eigenstates of the Hamiltonian in the target, infinite dimensional Hilbert space.

Finding such a basis is complicated by Gauss law requirements and the involved interplay between the kinetic (or electric) and the potential (or magnetic) part of the Hamiltonian: the former dominates for large cou-

pling, the latter for small coupling. In consequence, for large coupling it is efficient to work in an eigenbasis of the momentum operators and apply a cut-off at a certain momentum value. This approach yields the electric basis or, more generally, the Clebsch-Gordan expansion [4]. For small coupling, on the other hand, there exists an efficient magnetic basis in Abelian U(1) gauge theories [5, 6], but there is nothing equivalent know for non-Abelian SU(N) gauge theories.

Rather than considering the extreme regimes of the Hamiltonian, one can also choose to discretise the gauge group manifold itself [7–9]. This ansatz is equivalent to choosing a maximally localised functional basis, that is a finite number of Dirac δ functions. Of course, other functional bases are, in principle, be valid as well.

Using ideas from Ref. [10], we have found a functional basis that interpolates smoothly between both regimes. It is obtained using the eigenstates of the single plaquette Hamiltonian as a basis. Here, we present the explicit results for U(1) and SU(2), but the concept generalises easily to other gauge groups. While completing this work, we learned at a workshop at ECT* [11] of a simultaneous independent derivation of the same basis, very recently published in Ref. [12]. Consistently with the observations in Ref. [12], we find the single plaquette basis to be very efficient not only in the small coupling limit. In our U(1) and SU(2) simulations, the proposed basis allowed us to

work with system sizes significantly larger than previously feasible in tensor network simulations. Even three spatial dimensions can be approached.

In this work, we present an overview over the different bases. We benchmark them for multiple system sizes and a vast range of coupling strengths using tensor network states. The results are verified using exact diagonalisation and Green's function Monte Carlo whenever possible. In addition to the ground state energy and plaquette expectation value, we in particular compute the mass gap for a wide range of coupling-values, providing a considerably less forgiving stress test.

The rest of this paper is structured as follows: In Section II, we introduce the Hamiltonian formulation of lattice gauge theories. Then the different digitisation schemes are introduced first for U(1) in Section III and then for SU(2) in Section IV. Our results are presented in Section V and we conclude in Section VI.

II. THEORY

The Hamiltonian formulation of lattice gauge theories was first proposed by Kogut and Susskind in 1974 [3]. Similar to Wilson's famous Lagrangian formulation [13] it is also defined on a cubical lattice. Contrary its Lagrangian counterpart, only the spatial dimensions are discretised, while time is kept continuous. The gauge degrees of freedom are implemented as links connecting the spatial lattice sites. Each link is classically described by a colour matrix U, typically in the fundamental representation of the gauge group G.

Quantum states of the system are described by a many body wave function

$$\psi(\dots, U_{\mathbf{x}.k}, \dots) : G^{N_{\text{links}}} \to \mathbb{C},$$
 (1)

assigning a complex probability amplitude to every classical configuration $\{U_{\mathbf{x},k}\}$ of the gauge links. Directions and positions of each link are labelled by coordinate \mathbf{x} and direction k.

A. Operators

We begin by defining the position and momentum operators of the theory. Similar to regular quantum mechanics the position or link operators modify the wave function, by multiplication with the respective gauge degree of freedom. More precisely

$$\hat{U}_{\mathbf{x},k} \, \psi = U_{\mathbf{x},k} \, \psi \left(\dots, U_{\mathbf{x},k}, \dots \right) \,. \tag{2}$$

From this the plaquette operator can be constructed. It is defined as

$$\hat{P}_{\mathbf{x},ij} = \hat{U}_{\mathbf{x},i} \hat{U}_{\mathbf{x}+a\hat{\mathbf{i}},j} \hat{U}^{\dagger}_{\mathbf{x}+a\hat{\mathbf{j}},i} \hat{U}^{\dagger}_{\mathbf{x},j}$$
(3)

and can be understood as the oriented loop around a fundamental square of the lattice in the i j plane, starting and ending at position \mathbf{x} .

The momentum operators take the shape of Lie derivatives on the gauge group. In non-Abelian gauge groups there are left and right momentum operators $\hat{L}_{\mathbf{x},k}^c$ and $\hat{R}_{\mathbf{x},k}^c$ defined as

$$\hat{L}_{\mathbf{x},k}^{c} \psi = -i \frac{\mathrm{d}}{\mathrm{d}\beta} \psi \left(\dots, e^{-i\beta\tau_{c}} U_{\mathbf{x},k}, \dots \right) |_{\beta=0}$$
 (4)

and

$$\hat{R}_{\mathbf{x},k}^{c} \psi = -i \frac{\mathrm{d}}{\mathrm{d}\beta} \psi \left(\dots, U_{\mathbf{x},k} e^{i\beta\tau_{c}}, \dots \right) |_{\beta=0}.$$
 (5)

Here τ_c denote the generators of the Lie algebra in colour space. In a U(1) Abelian gauge group one has $\hat{L} = \hat{R}$. Similar to quantum mechanics, the link and momentum

Similar to quantum mechanics, the link and momentum operators are characterised by their commutation relations. These are given as

$$[\hat{L}_{\mathbf{x},i}^c, \hat{U}_{\mathbf{y},j}] = -\delta_{\mathbf{x}\mathbf{y}} \, \delta_{ij} \, t_c \, \hat{U}_{\mathbf{x},i} \,, \tag{6}$$

$$[\hat{R}_{\mathbf{x},i}^c, \hat{U}_{\mathbf{y},j}] = \delta_{\mathbf{x}\mathbf{y}} \, \delta_{ij} \, \hat{U}_{\mathbf{x},i} \, t_c \,. \tag{7}$$

For non-Abelian gauge groups the momentum operators also have non-trivial commutation relations with each other. These read

$$[\hat{L}_{\mathbf{x},i}^a, \hat{L}_{\mathbf{y},j}^b] = i f_{abc} \, \delta_{\mathbf{x}\mathbf{y}} \, \delta_{ij} \, \hat{L}^c \tag{8}$$

$$[\hat{R}_{\mathbf{x},i}^{a}, \hat{R}_{\mathbf{y},j}^{b}] = i f_{abc} \, \delta_{\mathbf{x}\mathbf{y}} \, \delta_{ij} \, \hat{R}^{c} \,. \tag{9}$$

Here f_{abc} are the structure constants of the gauge group. The commutator of left and right momentum operators vanishes.

B. The Hamiltonian

With these operators we can now define the Kogut-Susskind Hamiltonian. It reads

$$\hat{H} = \frac{g^2}{2} \sum_{\mathbf{x}, c, k} \left(\hat{L}_{\mathbf{x}, k}^c \right)^2 + \frac{N}{g^2} \sum_{\mathbf{x}, j < i} \operatorname{Tr} \left[\mathbb{1} - \operatorname{Re} \hat{P}_{\mathbf{x}, ij} \right].$$
(10)

Here N is the degree or number of colours of the unitary gauge group G. Note that the prefactor in front of the second (magnetic) term is a convention, with many different choices found across the literature.

The physical Hilbert space of the theory is further restricted by a constraint referred to as Gauss's law. It states that any physical state $|\psi\rangle$ needs to satisfy

$$\hat{G}_{\mathbf{x}}^{c} |\psi\rangle = \sum_{k} \left(\hat{L}_{\mathbf{x},k}^{c} + \hat{R}_{\mathbf{x}-a\hat{\mathbf{k}},k}^{c} \right) |\psi\rangle = 0.$$
 (11)

It implements local colour charge conservation at each vertex in the lattice.

The first term of the Hamiltonian is commonly referred to as the electric term. It contains a sum of Laplace-Beltrami operators $\sum_c (\hat{L}^c)^2$ applied to each gauge degree of freedom of the theory. It is therefore similar to the kinetic term in a many particle Hamiltonian in quantum mechanics. The second term is referred to as the magnetic term. It contains the sum over all plaquettes and thus implements a four particle nearest neighbour interaction.

At small values of the coupling g^2 the latter interaction dominates the dynamics of the theory and leads to strong entanglement between the four links of each plaquette. This entanglement makes efficient numerical simulations in this region extremely difficult. As the interaction does not constrain the wave function of any individual gauge link, naïve simulations that digitise in terms of single links basis, introduce non-localities in the electric Hamiltonian, and in turn a diverging basis sizes for $g^2 \to 0$ to produce accurate results.

C. Dual Formulation

One strategy to address the non-localities discussed above is to reparametrise the Hamiltonian, such that the magnetic term becomes local. For U(1) such formulations exist and are commonly used [5, 14, 15]. In the following we will go with the rotor formulation presented in [5]. Its Hamiltonian is given by

$$\hat{H}_{\text{dual}} = \frac{g^2}{2} \sum_{\mathbf{x},i} \left(\hat{L}_{\mathbf{x}} - \hat{L}_{\mathbf{x}+a\hat{\mathbf{i}}} \right)^2 + \frac{1}{2g^2} \sum_{\mathbf{x}} \left(2 - \hat{U}_{\mathbf{x}} - \hat{U}_{\mathbf{x}}^{\dagger} \right) . \tag{12}$$

After this reparametrization no Gauss law constraint is needed.

In the case of non-Abelian gauge groups the situation is less clear. While candidates for dual Hamiltonians exist [10, 16], they typically lead to long range electric interactions. These are problematic for some of the novel simulation methods proposed for Hamiltonian lattice gauge theories. In quantum computers such terms would lead to a higher demand in terms of swap gates, and tensor network methods typically work most efficiently with nearest neighbour Hamiltonians. At the time of writing it is unclear, whether a dual formulation with only local electric interaction exists for the non-Abelian case.

In the following we will run our non-Abelian tests on a 3×3 lattice with open boundary conditions. This system can be reparametrised in terms of four plaquette degrees of freedom anchored at the central vertex (see fig. 1). Dynamics on the eight remaining string degrees of freedom are prohibited by Gauss law. The resulting Hamiltonian

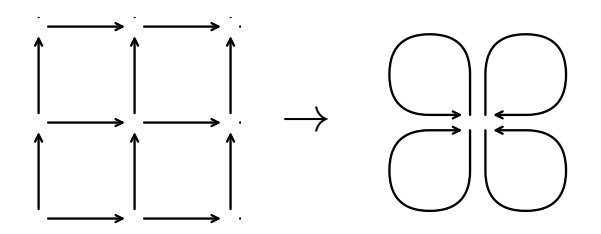


FIG. 1: Sketch of the 3×3 system in the original formulation on the left and the dual formulation on the right.

reads

$$\hat{H}_{3\times3} = 2g^2 \sum_{i=1}^4 \sum_{c=1}^3 \left(\hat{L}_i^c\right)^2 + g^2 \sum_{c=1}^3 \left(\hat{L}_1^c \hat{L}_2^c + \hat{L}_3^c \hat{L}_4^c + \hat{R}_1^c \hat{R}_3^c + \hat{R}_2^c \hat{R}_4^c\right) + \frac{2}{g^2} \sum_{i=1}^4 \text{Tr} \left[\mathbb{1} - \hat{U}_i\right].$$
(13)

The one remaining Gauss law constraint reads

$$\hat{G}^{c} |\psi\rangle = \sum_{i=1}^{4} \left(\hat{L}_{i}^{c} + \hat{R}_{i}^{c} \right) |\psi\rangle = 0.$$
 (14)

In our simulations we will enforce it via the addition of a penalty term

$$\hat{H}_{\text{penalty}} = \kappa \sum_{c} \left(\hat{G}^{c} \right)^{2} \tag{15}$$

where κ is a large positive real number.

III. DIGITISATION APPROACHES FOR U(1)

To run numerical simulations of the theory we need to first digitise the Hilbert space of functions

$$\psi: G^{N_{\mathrm{links}}} \to \mathbb{C}$$
 (16)

where G is the gauge group of the theory. To do so we begin with a local basis $\hat{\phi}_n$ for the space of functions

$$\psi: G \to \mathbb{C}$$
 (17)

Then one can take products of these functions to obtain a basis of the full subspace

$$|n_1, \dots, n_{N_{\text{links}}}\rangle = \prod_{i=1}^{N_{\text{links}}} \hat{\phi}_{n_i}$$
 (18)

In the following we will present several choices for these basis functions for U(1) and SU(2). Then we will test them in numerical simulations.

We begin with U(1). To give explicit forms of the single link basis states first we introduce a parametrization of the group:

$$U(\varphi) = e^{i\varphi}, \quad \varphi \in (-\pi, \pi].$$
 (19)

A. Electric Basis Operators

The most common choice of basis functions is given by

$$\hat{\phi}_{\text{el.}}^m(\varphi) = \frac{1}{2\pi} e^{i \, m\varphi} \,, \quad m \in \mathbb{Z} \,.$$
 (20)

In this basis the electric operator is diagonal

$$\langle m | L | n \rangle = m \, \delta_{m,n},\tag{21}$$

hence it's called the electric basis. The link operator takes the shape of a ladder operator:

$$\langle m|U|n\rangle = \delta_{m,n+1} \tag{22}$$

To obtain finite operators one truncates by only considering states for which $|m| \leq m_{\text{max}}$. This will then give operators of dimension $d_{\text{op}} = 2m_{\text{max}} + 1$.

As the electric basis functions are the low-lying eigenstates of the electric Hamiltonian they perform very well at large values of the coupling g^2 . In the limit $g^2 \to 0$, i.e. the continuum limit of the theory, an ever-increasing number of states is needed to achieve accurate results.

B. Magnetic Basis Operators

One way to address this are the magnetic basis operators proposed in [6]. Here first the link operators are modified to be the ones of a $Z_{2\ell+1}$ subgroup of U(1):

$$U|n\rangle \to \mathcal{U}|m\rangle = \begin{cases} |-m\rangle & m+1=\ell\\ |m+1\rangle & \text{otherwise} \end{cases}$$
 (23)

Then one can define a discrete Fourier-transform in the form of

$$\mathcal{F} = \frac{1}{\sqrt{2\ell+1}} \sum_{\mu,\nu=-\ell}^{\ell} \exp\left(\frac{2\pi i \mu \nu}{2\ell+1}\right) |\mu\rangle \langle \nu| . \qquad (24)$$

Once applying this transformation the link operator becomes diagonal:

$$\mathcal{FUF}^{\dagger} = \sum_{\mu=-\ell}^{\ell} \exp\left(-\frac{2\pi i \mu}{2\ell+1}\right) |\mu\rangle \langle \mu| \qquad (25)$$

To then gain a computational advantage towards weak couplings, one can then truncate the transformed operator to only contain the states where \mathcal{FUF}^{\dagger} is sufficiently close to 1. This is done, because the wave function is expected to vanish for configurations where $\mathcal{FUF}^{\dagger} \neq 1$ at weak couplings.

This is equivalent to modifying the Fourier transformation to read

$$\tilde{\mathcal{F}} = \frac{1}{\sqrt{2\ell+1}} \sum_{\mu=-n_{\text{max}}}^{n_{\text{max}}} \sum_{\nu=-\ell}^{\ell} \exp\left(\frac{2\pi i \mu \nu}{2\ell+1}\right) |\mu\rangle \langle \nu| , (26)$$

where $n_{\text{max}} \leq \ell$ and relates to the actual operator dimension again as $d_{\text{op}} = 2n_{\text{max}} + 1$.

To obtain accurate results the integer parameter ℓ needs to be tuned for a given operator dimension and coupling. In the following we pick ℓ such that it minimises the error of the ground state energy of a single plaquette system.

While more elaborate tuning schemes are certainly conceivable, we will show that this produced optimal results for the system sizes and observables considered in this article.

C. Plaquette State Basis

Lastly we will propose a functional basis for U(1) LGTs, which we call plaquette state basis (see also Ref. [12] for an independent derivation). For this we start by studying a single plaquette in pure gauge theory. In the dual formulation the Hamiltonian is given by:

$$\hat{H}_{SP} = -2g^2 \frac{d^2}{d\varphi_P^2} + \frac{1}{g^2} (1 - \cos \varphi_P)$$
 (27)

To calculate its eigenstates one has to solve the stationary Schrödinger equation given by:

$$\hat{H}_{\rm SP} |\psi_n\rangle = E_n |\psi_n\rangle$$
 (28)

Plugging in the Hamiltonian we thus end up with a differential equation of the form

$$\left(-\frac{\mathrm{d}^2}{\mathrm{d}\varphi^2} + \frac{1}{2g^4}\left(1 - \cos\varphi\right) - \frac{E_n}{2g^2}\right)\psi_n(\varphi) = 0. \quad (29)$$

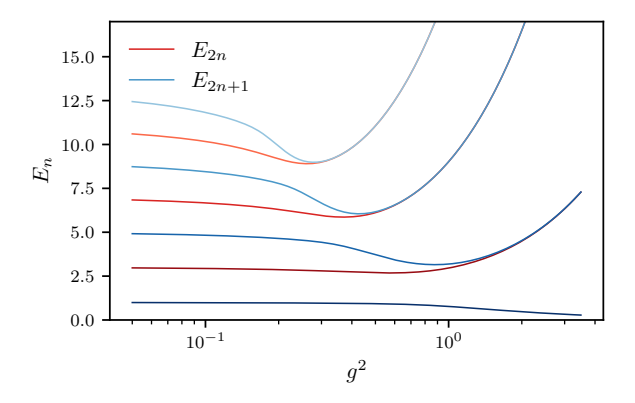
This equation is known as Mathieu's differential equation [17]. In its canonical form it reads

$$y(x)'' + (\lambda - 2q\cos(2x))y = 0.$$
 (30)

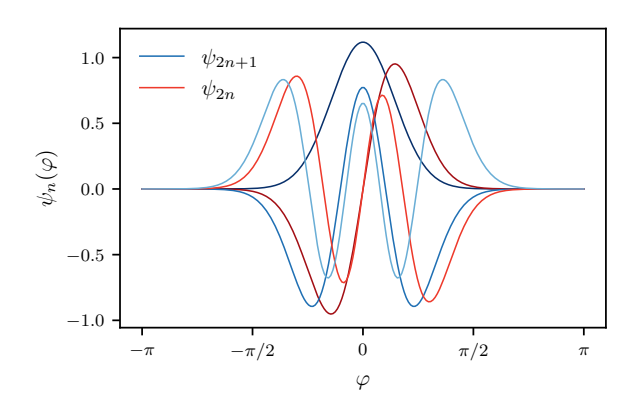
To bring eq. (29) into this form we first need to reparametrise $\varphi \to 2x$. Then we can read of

$$q = -\frac{1}{g^4}$$
 and $\lambda = \frac{2E_n}{g^2} - \frac{2}{g^4}$. (31)

The solutions of this equation are periodic solution, whenever λ is equal to one of the Mathieu characteristic numbers $a_n(q)$ or $b_n(q)$. Due to the periodicity of



(a) The low energy spectrum of the single plaquette system as a function of the coupling g^2 .



(b) The wave functions corresponding to the single plaquette eigenstates at a fixed coupling of $g^2 = 0.1$.

FIG. 2: Spectrum and eigenstates of the single plaquette system.

Solution	Parity	Period
ce_{2n}	even	π
ce_{2n+1}	even	2π
se_{2n}	odd	π
se_{2n+1}	odd	2π

TABLE I: Solutions of the Mathieu equation.

the parametrization of the gauge group, only periodic solutions are of interest. Thus, the spectrum of the one plaquette system is given by

$$E_n = \frac{\lambda g^2}{2} + \frac{1}{g^2} \,. \tag{32}$$

The corresponding eigenfunctions are denoted as se_n and ce_n and are called the sine- and cosine-elliptic functions respectively. They can be classified by periodicity and parity according to table I. As our parametrization defined in eq. (19) has a period of π (after the reparametrization) only the π periodic solutions are valid eigenstates of the system.

We plot the single plaquette spectrum in fig. 2a and show the corresponding eigenstates at a coupling of $g^2 = 0.1$ in fig. 2b. (Describe this a bit more)

A complete set of basis functions is thus given by

$$\psi_n(\varphi) = \begin{cases} \frac{1}{\sqrt{\pi}} \operatorname{ce}_{n+1}(2\varphi) & n \text{ odd,} \\ \frac{1}{\sqrt{\pi}} \operatorname{se}_n(2\varphi) & n \text{ even.} \end{cases}$$
(33)

To obtain a finite basis needed for simulations we once again truncate by imposing $n \leq 2n_{\text{max}} + 1$. The operators are obtained by numerically solving the integrals

$$\mathcal{O}_{ij} = \langle \psi_i | \mathcal{O} | \psi_j \rangle = \int_0^{2\pi} d\varphi \, \overline{\psi_i}(\varphi) \, \mathcal{O} \, \psi_j(\varphi) \,. \tag{34}$$

It is possible that analytical solutions to these integrals exist. However, for now we will leave their derivation to future researchers.

Note that that squared operators, such as \hat{L}^2 were integrated out separately and not simply taken as the matrix squared of the \hat{L} operator. This is done, because \hat{L} does not preserve the subspace of basis functions. Thus, we expect more accurate results, when treating \hat{L}^2 as an independent operator.

IV. DIGITISATION APPROACHES FOR SU(2)

Next we will show how some of these approaches translate to the non-Abelian case of SU(2).

A. Clebsch-Gordan Expansion

Here the equivalent of the electric basis operators was first formulated in [18]. The electric eigenstates are labelled by their eigenvalues with respect to the Laplace Beltrami operator $\sum_c (\hat{L}^c)^2$, as well as one of the left and right momentum operators. Here typically \hat{L}^3 and \hat{R}^3 are chosen. This gives a set of states

$$|j, m_L, m_R\rangle$$
, $j \in \mathbb{N}/2$, $m_L, m_R \in \{-j, -j+1, \dots, j-1, j\}$, (35)

which obey

$$\sum_{c} (\hat{L}^{c})^{2} |j, m_{L}, m_{R}\rangle = j(j+1) |j, m_{L}, m_{R}\rangle$$
 (36)

$$\hat{L}^3 |j, m_L, m_R\rangle = m_L |j, m_L, m_R\rangle \tag{37}$$

and

$$\hat{R}^3 |j, m_L, m_R\rangle = -m_R |j, m_L, m_R\rangle . \tag{38}$$

The action of \hat{L}^1 and \hat{L}^2 can be defined in terms of raising and lowering operators

$$(\hat{L}^{1} \pm i \hat{L}^{2}) |j, m_{L}, m_{R}\rangle$$

$$= \sqrt{j(j+1) - m_{L}(m_{L} \pm 1)} |j, m_{L} \pm 1, m_{R}\rangle.$$
(39)

Similarly, \hat{R}^1 and \hat{R}^2 obey

$$(\hat{R}^{1} \mp i \, \hat{R}^{2}) |j, m_{L}, m_{R}\rangle$$

$$= -\sqrt{j(j+1) - m_{R}(m_{R} \pm 1)} |j, m_{L}, m_{R} \pm 1\rangle .$$
(40)

Lastly the link operators need to be obtained. This is done via a Clebsch-Gordan (CG) expansion [18]:

$$U_{c_{1}c_{2}} = \sum_{j,m_{L},m_{R}} \sum_{j',m_{L'},m_{R'}} \sqrt{\frac{2j+1}{2j'+1}} \times \langle j m_{L}, 1/2 m_{1} | j' m_{L'} \rangle \langle j' m_{R'} | j m_{R}, 1/2 m_{2} \rangle$$

$$|j' m_{L'} m_{R'} \rangle \langle j m_{L} m_{R} |,$$
(41)

where the colour indices c_1, c_2 correspond to m_1, m_2 according to the following convention: $m_i = 1/2 - c_i$.

The resulting operators couple states with the main quantum number j to states with $j' = j \pm 1/2$. Overall these operators fulfil all the previously stated commutations relations exactly. However, similarly to the electric operators in U(1) they fail to capture the weak coupling regime of the theory.

B. Plaquette State Basis

This can again be solved by considering the states of a single plaquette. Its Hamiltonian reads

$$\hat{H}_{SP} = 2g^2 \sum_{c} (\hat{L}^c)^2 + \frac{4}{g^2} (1 - \cos \rho) .$$
 (42)

The angles ρ , θ and φ parametrise the SU(2) gauge group, where a group element U is given by

$$U(\rho, \theta, \varphi) = \cos \rho \, \mathbb{1} - i \sin \rho \, \vec{n}(\theta, \varphi) \cdot \vec{\sigma} \tag{43}$$

with

$$\vec{n}(\theta,\varphi) = \begin{pmatrix} \sin\theta\cos\varphi\\ \sin\theta\sin\varphi\\ \cos\phi \end{pmatrix}. \tag{44}$$

In these coordinates $\sum_c \left(\hat{L}^c\right)^2$ takes the shape of the Laplace-Beltrami operator on the group manifold:

$$\sum_{c} (\hat{L}^{c})^{2} = -\frac{1}{4\sin^{2}\rho} \left(\frac{\partial}{\partial\rho} \left(\sin^{2}\rho \frac{\partial}{\partial\rho} \right) + \Delta_{S_{2}} \right)$$
(45)

Here Δ_{S_2} is the Laplace Beltrami Operator on the 2-sphere in terms of the spherical coordinates θ and φ . Therefore, we can make a separation Ansatz:

$$\phi_n(\rho, \theta, \varphi) = \frac{u(\rho)}{\sin \rho} Y(\theta, \varphi)$$
 (46)

The spherical part is solved by the spherical Harmonics Y_{lm} which fulfil

$$\Delta_{S_2} Y_{lm} = l(l+1)Y_{lm} \,. \tag{47}$$

This then leads to the radial equation given by

$$u'' + \left(1 - \frac{8}{g^4} \left(1 - \cos \rho\right) + \frac{2E_n}{g^2} + \frac{l(l+1)}{\sin^2 \rho}\right) u = 0.$$
 (48)

For the gauge invariant case, i.e. l=0 this again reduces to the Mathieu equation. Solutions again need to have a period of π . Additionally, only symmetric solutions are differentiable at the poles. As the additional quotient of $\sin \rho$ itself is anti-symmetric only anti-symmetric solutions of the Mathieu equations can be considered.

After reparametrization from $\rho \to 2x$ we can identify the coefficients of the Mathieu equation to be

$$q = -\frac{16}{g^4}$$
 and $\lambda = 4 + \frac{8E_n}{g^2} - \frac{32}{g^4}$. (49)

With this we can write down a set of orthonormal basis states as

$$\hat{\phi}_{nlm}(\rho,\theta,\varphi) = \frac{\text{se}_{2n+2}(q;\rho/2)}{\sin\rho} Y_{lm}(\theta,\varphi).$$
 (50)

Note that while these functions are an orthonormal basis of the Hilbert space, they are only the eigenfunctions of the single plaquette system for l=0. To fix this one would need to solve eq. (48) separately for $l\neq 0$. However, to the author's knowledge this can only be done numerically. The actual set of eigenfunctions is likely to perform much better, as suggested in [16].

To obtain finite operators we again truncate. In this case this is done by imposing $l \leq l_{\text{max}}$ and $n \leq n_{\text{max}}$ giving a total operator dimension of

$$d_{\rm Op} = (n_{\rm max} + 1)(l_{\rm max} + 1)^2. \tag{51}$$

The operator matrices are then again obtained via numerical integration.

V. RESULTS

Next we want to test these operators in numerical simulations. To do so we use the ITensor DMRG algorithm[19]. This is done by mapping each $\mathrm{U}(1)$ rotor in our two-dimensional lattice onto the sites of a one dimensional MPS. More specifically the rotor found at lattice coordinate x and y is mapped to an MPS site position

$$i_{\text{MPS}} = x(L-1) + y.$$
 (52)

This way we will eventually still encounter an exponential slow down, when increasing the system size in the y direction, but get much better scaling in the x direction. So while certainly not efficient for larger two-dimensional systems, it allows us to explore significantly larger system sizes, than with a regular Eigensolver.

The SVD cutoff parameters and energy convergence criteria in ITensor were tuned such that we are confident that the finite bond dimension is not contributing a significant error in the following results. It should thus just be viewed as more memory efficient Eigensolver for sparse systems with local interactions. Nevertheless, more appropriate tensor network algorithms will be needed in the future to explore larger system sizes efficiently.

Furthermore, we will compare the digitised Hamiltonian results to results obtained from Green's function Monte Carlo (GFMC) Methods. For details on this algorithm, please refer to section A. In short one can obtain good estimates of the ground state energy and ground state plaquette expectation value.

A. U(1) Results

To begin our numerical tests we study a 4×4 system, with open boundary conditions in the dual U(1) formulation. This system contains 9 rotor degrees of freedom. Thus, it should contain enough rotor interactions of the full theory to give a realistic benchmark, while keeping the overall computational costs manageable.

In fig. 3 we plot the ground state energy E_0 and ground state plaquette expectation value P as a function of the coupling g^2 . Shown are results for the electric basis operators in red, the magnetic basis operators in orange and the plaquette state operators in blue. For all operators the truncation was chosen such that $d_{\rm Op}=5$. For comparison, we also include Green's function Monte Carlo (GFMC) results, plotted as the black crosses, as well as a simulation of the original Kogut-Susskind Hamiltonian with electric operators also truncated at $d_{\rm Op}=5$.

As expected both simulations using the electric operators quickly diverge from the GFMC results when decreasing the coupling, while the magnetic and plaquette state operators stay closely match the GFMC results at all couplings. As can be seen in the zoomed in panel, the magnetic basis functions oscillate around the GFMC results. Each jump in this zig-zag pattern corresponds to a change in the value of ℓ when tuning for a given coupling and operator dimension. The plaquette state operators do not show this behaviour and thus lead to much smaller deviations from the reference results.

Next, we study the mass gap $M = E_1 - E_0$. While it possible to extract mass gaps from Green's function Monte-Carlo simulations [20], we did not manage to achieve satisfactory precision in our implementation. Therefore, we only show the electric simulation of the original Hamilto-

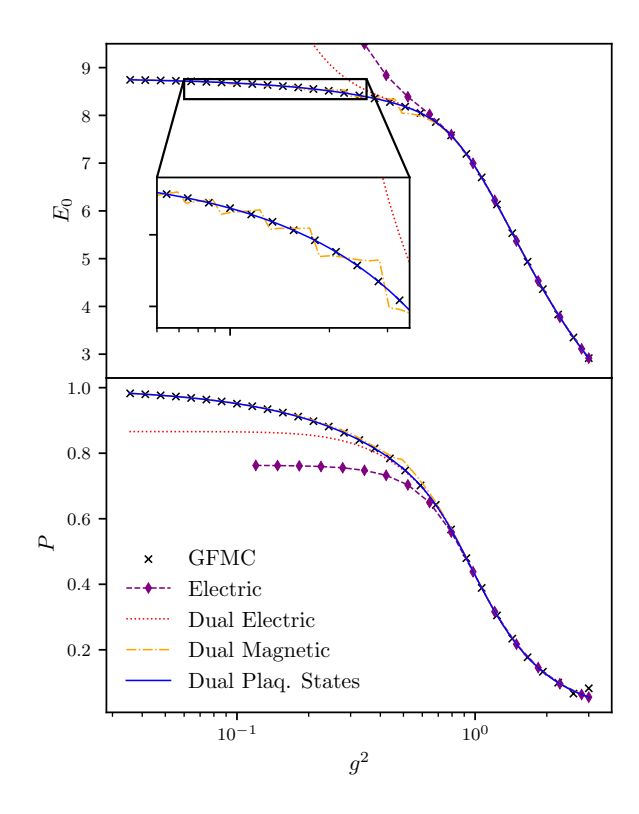


FIG. 3: The ground state energy (top) and ground state plaquette expectation value (bottom) as a function of the coupling g^2 for a 4×4 system with U(1) gauge. This is done for the original Kogut-Susskind Hamiltonian using electric basis operators (purple), and for the dual formulation using electric (red), magnetic (orange) and plaquette state operators (blue). All truncations are chosen such that $d_{\rm op} = 5$. Their results are compared to GFMC results shown by the black crosses.

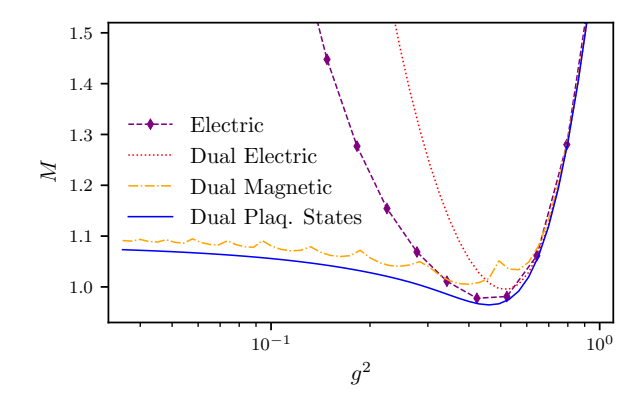


FIG. 4: The mass gap M as a function of the coupling g^2 for the same system and operators as fig. 3.

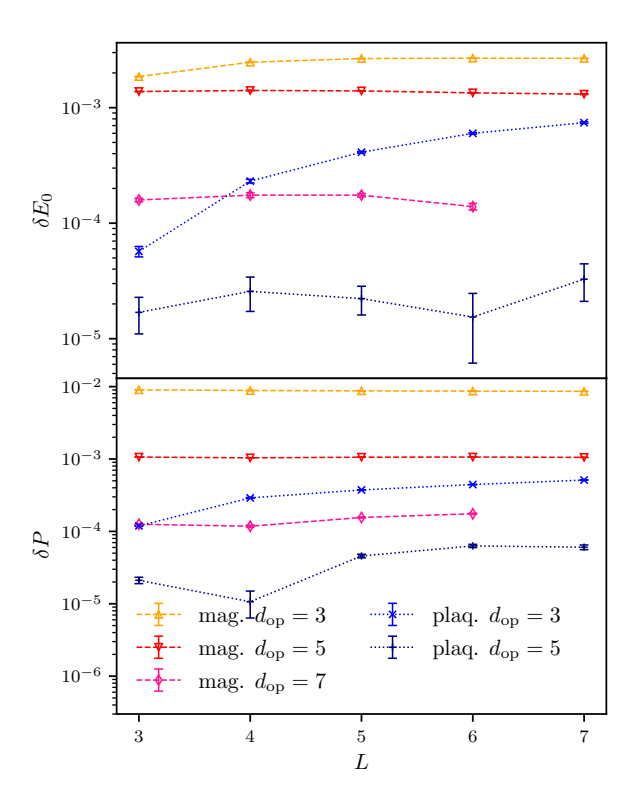


FIG. 5: The relative deviations of the ground state energy (top) and the plaquette expectation value (bottom) at a coupling of $g^2 = 0.1$ as a function of the system size L. This is done for magnetic operators at three different truncations (orange, red, pink) and for plaquette state operators at two different truncations (blue, navy).

nian as well as the three simulations of the dual Hamiltonian in fig. 4. The operators are again truncated such that $d_{\rm Op}=5$.

The behaviour of M as a function of the coupling is qualitatively quite similar to the ground state observables. Both electric formulations again diverge towards small couplings, while the magnetic basis and plaquette state basis operators again are stable in the weak coupling limits. The plaquette states give a marginally smaller mass gap, and the magnetic basis states again show sharp transitions, when changing ℓ .

To get a more quantitative idea of the accuracy of the different operators we study the relative deviations from the GFMC results. We define the relative deviation $\delta \mathcal{O}$ of an observable \mathcal{O} as

$$\delta \mathcal{O} = \left| \frac{\mathcal{O}_{\text{measured}} - \mathcal{O}_{\text{ref}}}{\mathcal{O}_{\text{ref}}} \right| . \tag{53}$$

In fig. 5 we plot the relative deviations with respect to the GFMC results of E_0 and P at a fixed coupling of $g^2 = 0.1$ as a function of the lattice size L.

This provides insights into how our results for the

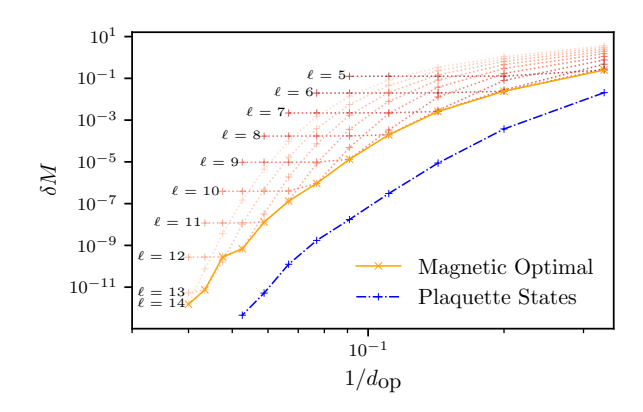


FIG. 6: The relative deviation of the mass gap δM , with respect to the result at $d_{\rm op}=33$, shown as a function of the inverse operator dimension $d_{\rm op}^{-1}$ for a 4×4 system at a coupling of $g^2=0.1$. In blue, we show results for the plaquette state operators, while the orange points are results obtained from the magnetic operators with optimal ℓ . The cloud of dashed lines above the orange line shows other possible choices of the ℓ parameter of the magnetic operators.

small system sizes compare to more substantial volumes. Shown in orange, red and pink are magnetic operators of with operator dimensions of 3, 5, and 7. The blue and dark blue points are plaquette state operators of dimension 3 and 5.

Similarly to the previous results, the plaquette states show much lower deviations, than the magnetic operators. For both deviations decrease, when increasing the operator dimension. The smallest deviation reached by increasing the operator dimension, seems to be around 10^{-5} for both the ground state energy and the plaquette expectation value. It is likely that the constraining factor here are unaddressed systematics in the GFMC results. For a more detailed discussion of these refer to section A. Neither of the operators show a strong volume depen-

dence. The most pronounced effect is visible for the smallest truncations in both approaches. Here, the deviations in the energy increase by about one order of magnitude from the smallest to the largest lattice. For the larger truncations the deviations are mostly independent of the volume. This leaves us hopeful that the proposed operators will also perform well in larger simulations.

Lastly we want to get an impression of the convergence behaviour of the mass gap. For this we will compare to a high resolution plaquette state result at $d_{\rm op}=33$ to results obtained with smaller truncation at a coupling of $g^2=0.1$.

The results are depicted in fig. 6. Here we plot the relative deviation δM of the reference Mass as a function of the inverse operator dimension for the plaquette state operators in blue. Additionally, results for the magnetic basis operators are shown. For the red line ℓ was chosen

such that the error of the single plaquette ground state energy is minimised for a given n_{max} . The dotted orange lines show other possible choices for ℓ .

Overall the plaquette states show between two and three orders of magnitude less deviation from the reference result at fixed operator dimension when compared to the best magnetic basis operators. However, both methods converge to the reference result, and no significant difference in the convergence rate can be observed.

Furthermore, the proposed criterion for tuning ℓ in the magnetic basis operators seems to give optimal results. This can be seen, as the orange line obtained from tuned magnetic basis operators bounds the cloud of all possible magnetic basis operators from below. It is possible that this only holds at small system sizes, and different methods are needed for larger systems.

Next, we applied the plaquette state basis for simulations of U(1) LGT in three spatial dimensions, using the same snake MPS solver as before with adapted mapping eq. (52). This represents likely a situation where the limits of snake MPS are tested, which is why we could simulate a 2×3^2 system only. The corresponding results are shown in fig. 7, where we again compare to GFMC results. Overall deviations seem significantly larger than in the two-dimensional case for comparable d_{op} , which can be understood by the larger number of interaction terms in the Hamiltonian. Nevertheless, with a small number of plaquette basis states a range of squared coupling values $g^2 \in [5 \cdot 10^{-2}, 2.5]$ can be simulated with small deviations to the GFMC result. We take this as a strong indication that the plaquette state basis can enable simulations in three spatial dimensions without large truncation effects.

B. SU(2) Results

Finally, we would like to present some results for SU(2). Here we study the 3×3 system described by the Hamiltonian given in eq. (13). Gauss law is enforced via the described penalty term. $\kappa=10$ proved to be large enough to filter the physical states of interest. This can be checked, by ensuring that the expectation value of the penalty Hamiltonian vanishes.

In fig. 8 we again plot the ground state energy and plaquette expectation value as a function of the coupling g^2 . Shown are results for Clebsch-Gordan operators truncated at $J_{\rm max} \leq 2$ ($d_{\rm op} = 55$) in purple, and for the plaquette state operators at three different truncations. They have operator dimensions of 8, 12 and 45 respectively. Once again we compare them to GFMC results. Similar to the results for U(1), the Clebsch-Gordan operators eventually diverge towards small couplings, while the plaquette state operators again match the GFMC results well at all couplings.

The picture is less clear, when studying the mass gap. This is shown in fig. 9. Again we do not have a GFMC

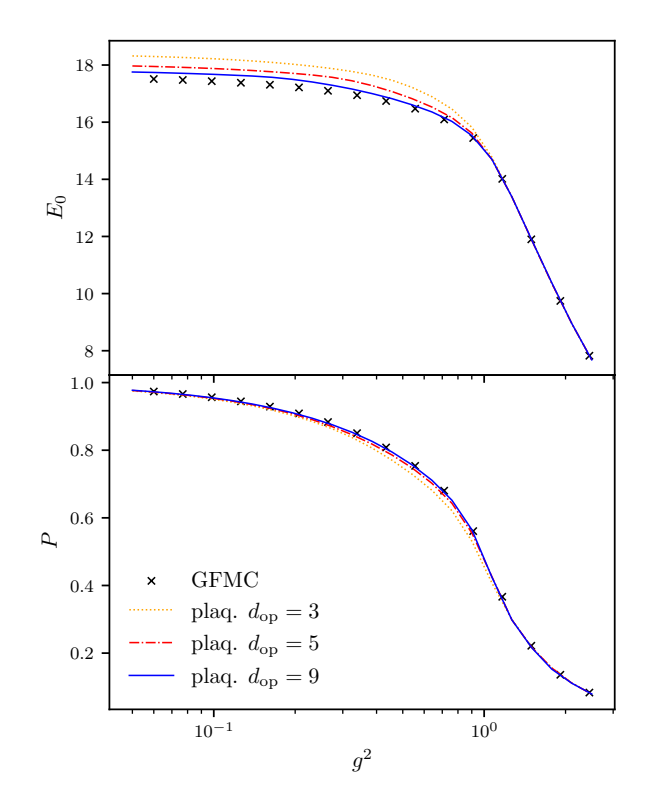


FIG. 7: The ground state energy and plaquette expectation value (like in fig. 3) for a three-dimensional system of size 2×3^2 as a function of the coupling. Shown are results for the plaquette states at three different truncations.

result to compare to. However, the rather large electric operators are expected to be reasonably accurate up to the point where they diverge at around $g^2 < 0.6$. We can clearly see that the plaquette state operators seem to converge towards the electric results at stronger coupling. This leaves us hopeful, that this approach will also deliver accurate results for SU(2) simulations at weak couplings.

VI. DISCUSSION AND CONCLUSION

The results presented in this work show that a functional basis constructed from the eigenstates of the single-plaquette Hamiltonian provides an efficient representation for Hamiltonian lattice gauge theories. The advantage of this approach, named the plaquette-state basis, is that it maintains a high accuracy at small values of the gauge coupling compared to the other truncation schemes tested.

For the Abelian U(1) theory, the plaquette-state basis exhibits a consistent and substantial reduction in error compared to both electric and magnetic bases at a fixed operator dimension. The improvement is particularly pronounced in the weak-coupling regime, where

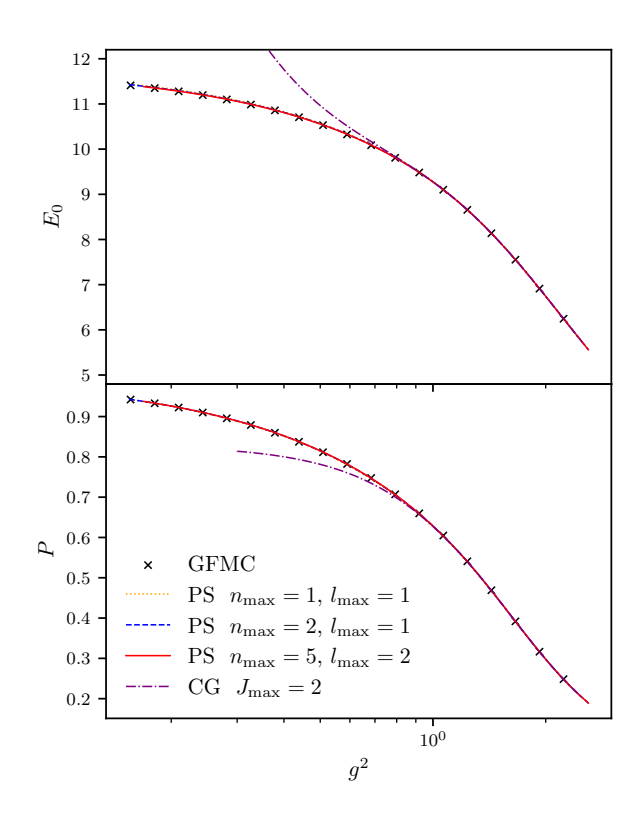


FIG. 8: The ground state energy and ground state plaquette expectation value as a function of the coupling for a 3×3 system of SU(2) gauge theory. This is done for the Clebsch-Gordan Operators with a truncation of $J_{\rm max}=2$ shown in purple and for three sets of plaquette state operators at different truncations in orange, blue and red respectively.

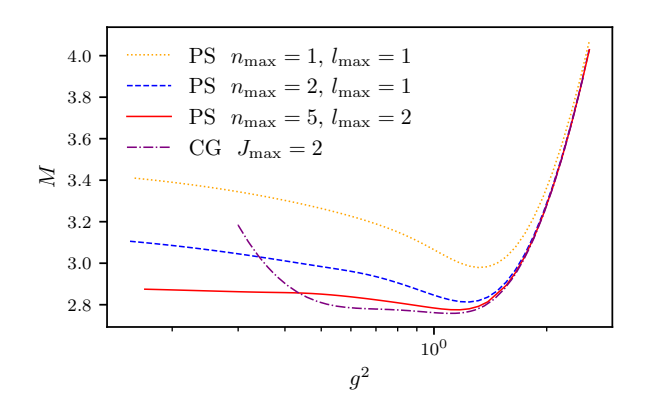


FIG. 9: The mass gap M for the system and operators plotted in fig. 8.

our results agree with GFMC calculations over the entire coupling range. Another advantage of the plaquette-state formulation is its versatility in accessing a wider range of observables. While GFMC provides highly accurate ground-state quantities, it is difficult to extract

excited-state properties such as the mass gap with satisfactory precision. Moreover, the plaquette-state basis shows no significant deterioration in accuracy up to the largest lattices simulated. These features suggest that the basis captures the relevant low-energy subspace of the Hamiltonian, offering a compact yet faithful digitisation for both tensor-network and quantum-computing applications.

The plaquette state basis appears to retain efficiency in three spatial dimensions, as our exploratory simulations in a 2×3^2 volume indicate. Here we are currently working on a GPU implementation which could enable simulations of larger three dimensional systems.

Preliminary investigations for the SU(2) case indicate that the same construction extends to non-Abelian gauge theories. The plaquette-state basis reproduces the available results for GFMC at strong and weak couplings keeping a higher versatility. An open challenge lies in formulating a local dual Hamiltonian for non-Abelian gauge theories. The lack of such a representation currently restricts simulations to relatively small lattices. A local formulation would enable the application of tensornetwork or quantum-computing algorithms to larger systems while retaining the advantages of the plaquette-state basis. Addressing this issue represents an important direction for future work.

It is worth mentioning that Green's function Monte Carlo represents a valuable tool which we used to verify our results for parameter values where no other method was applicable. It remains to be seen whether GFMC can also be applied for real time evolution or with a θ -term or baryon chemical potential.

The idea of constructing plaquette-based basis functions has recently attracted growing attention. During this work we became aware of the independent development of a closely related approach by P. Fontana and collaborators, presented in Refs. [12, 16]. Both projects appear to have originated from the insights of Bauer et al. [10], whose analysis provided many of the conceptual ingredients for the present method. Here we presented complementary results and insights, in particular more observables, three-dimensional simulations, and a comparison with other truncation schemes and GFMC.

The question of a suitable Hamiltonian for the non-Abelian case remains. At the time of writing no suitable local formulation is known. This is likely a necessity in order to extract non-trivial physical observables for larger scale Hamiltonian simulations.

ACKNOWLEDGMENTS

This project was funded by the Deutsche Forschungsgemeinschaft (DFG, German Research Foundation) as a project in the CRC 1639 NuMeriQS – project no. 511713970. We thank ECT* for support at the Workshop "Hamiltonian Lattice Gauge Theories: Status, Novel Developments and Applications" during which this work has been developed. This work is supported by the European Union's Horizon Europe Framework Programme (HORIZON) under the ERA Chair scheme with grant agreement no. 101087126. This work is supported with funds

from the Ministry of Science, Research and Culture of the State of Brandenburg within the Centre for Quantum Technologies and Applications (CQTA).



- Alberto Di Meglio et al., "Quantum Computing for High-Energy Physics: State of the Art and Challenges," PRX Quantum 5, 037001 (2024), arXiv:2307.03236 [quant-ph].
- [2] Giuseppe Magnifico, Giovanni Cataldi, Marco Rigobello, Peter Majcen, Daniel Jaschke, Pietro Silvi, and Simone Montangero, "Tensor networks for lattice gauge theories beyond one dimension," Commun. Phys. 8, 322 (2025), arXiv:2407.03058 [hep-lat].
- [3] John B. Kogut and Leonard Susskind, "Hamiltonian Formulation of Wilson's Lattice Gauge Theories," Phys. Rev. D 11, 395–408 (1975).
- [4] Erez Zohar and Michele Burrello, "Formulation of lattice gauge theories for quantum simulations," Phys. Rev. D 91, 054506 (2015), arXiv:1409.3085 [quant-ph].
- [5] Judah F. Unmuth-Yockey, "Gauge-invariant rotor hamiltonian from dual variables of 3d u(1) gauge theory," Phys. Rev. D 99, 074502 (2019).
- [6] Jan F. Haase, Luca Dellantonio, Alessio Celi, Danny Paulson, Angus Kan, Karl Jansen, and Christine A. Muschik, "A resource efficient approach for quantum and classical simulations of gauge theories in particle physics," Quantum 5, 393 (2021).
- [7] Tobias Hartung, Timo Jakobs, Karl Jansen, Johann Ostmeyer, and Carsten Urbach, "Digitising SU(2) gauge fields and the freezing transition," Eur. Phys. J. C 82, 237 (2022), arXiv:2201.09625 [hep-lat].
- [8] Timo Jakobs, Marco Garofalo, Tobias Hartung, Karl Jansen, Johann Ostmeyer, Dominik Rolfes, Simone Romiti, and Carsten Urbach, "Canonical momenta in digitized SU(2) lattice gauge theory: definition and free theory," Eur. Phys. J. C 83, 669 (2023), arXiv:2304.02322 [hep-lat].
- [9] Timo Jakobs, Marco Garofalo, Tobias Hartung, Karl Jansen, Johann Ostmeyer, Simone Romiti, and Carsten Urbach, "Dynamics in Hamiltonian Lattice Gauge Theory: Approaching the Continuum Limit with Partitionings of SU(2)," (2025), arXiv:2503.03397 [hep-lat].
- [10] Irian D'Andrea, Christian W. Bauer, Dorota M. Grabowska, and Marat Freytsis, "New basis for Hamiltonian SU(2) simulations," Phys. Rev. D 109, 074501 (2024), arXiv:2307.11829 [hep-ph].
- [11] C. Urbach, S. Romiti, E. R. Ortega, G. Magnifico, K. Jansen, and R. Lewis, "Hamiltonian Lattice Gauge Theories: Status, Novel Developments and Applications," (2025), ECT* Workshop, 1-5 Sept.
- [12] Marc Miranda-Riaza, Pierpaolo Fontana, and Alessio Celi, "Renormalized dual basis for scalable simulations of 2+1D compact quantum electrodynamics," (2025), arXiv:2510.18594 [quant-ph].
- [13] Kenneth G. Wilson, "Confinement of Quarks," Phys. Rev. D 10, 2445–2459 (1974).

- [14] Axel Weber, "U(1) gauge theory on a spatial lattice: Duality, photons, and shadow states," JHEP **05**, 157 (2013).
- [15] Jan F. Haase, Luca Dellantonio, Alessio Celi, Danny Paulson, Angus Kan, Karl Jansen, and Christine A. Muschik, "A resource efficient approach for quantum and classical simulations of gauge theories in particle physics," Quantum 5, 393 (2021), arXiv:2006.14160 [quant-ph].
- [16] Pierpaolo Fontana, Marc Miranda Riaza, and Alessio Celi, "Efficient Finite-Resource Formulation of Non-Abelian Lattice Gauge Theories beyond One Dimension," Phys. Rev. X 15, 031065 (2025), arXiv:2409.04441 [quant-ph].
- [17] Emile Mathieu, "Mémoire sur le mouvement vibratoire d'une membrane de forme elliptique." Journal de Mathématiques Pures et Appliquées 13, 137–203.
- [18] Erez Zohar and Michele Burrello, "Formulation of lattice gauge theories for quantum simulations," Phys. Rev. D 91, 054506 (2015).
- [19] Matthew Fishman, Steven R. White, and E. Miles Stoudenmire, "The ITensor Software Library for Tensor Network Calculations," SciPost Phys. Codebases, 4 (2022).
- [20] Chris J. Hamer, Robert J. Bursill, and Maria Samaras, "Green's function Monte Carlo study of correlation functions in the (2+1)-dimensions U(1) lattice gauge theory," Phys. Rev. D 62, 054511 (2000), arXiv:hep-lat/0002001.
- [21] M. H. Kalos, "Monte carlo calculations of the ground state of three- and four-body nuclei," Phys. Rev. 128, 1791–1795 (1962).
- [22] J. Carlson, "Green's function monte carlo study of light nuclei," Phys. Rev. C 36, 2026–2033 (1987).
- [23] S. A. Chin, O. S. van Roosmalen, E. A. Umland, and S. E. Koonin, "Exact ground-state properties of the su(2) hamiltonian lattice gauge theory," Phys. Rev. D 31, 3201–3212 (1985).
- [24] C. J. Hamer, M. Sheppeard, Zheng Weihong, and D. Schütte, "Universality for su(2) yang-mills theory in 2+1 dimensions," Phys. Rev. D 54, 2395–2398 (1996).
- [25] Khaldoon Ghanem, Niklas Liebermann, and Ali Alavi, "Population control bias and importance sampling in full configuration interaction quantum monte carlo," Phys. Rev. B 103, 155135 (2021).

Gauge Group τ_c	$ E_L $	$F_{Q\mathbf{x},i}^c$	σ_{χ}	$E_{ m physical}$
U(1) 1	$\left(2\alpha - \frac{2}{g^4}\right) \sum_{P} \cos \varphi_P$ $-\frac{1}{4} \sum_{\mathbf{x},i} F_{Q\mathbf{x},i}^2$	$\alpha \sum_{\mathbf{x},i} \sum_{P \ni U_{\mathbf{x},i}} s_P (U_{\mathbf{x},i}) \sin \varphi_P$	$\sqrt{2\Delta t}$	$\frac{g^2}{2} \left(E_L + \frac{2}{g^2} N_{\text{plaquettes}} \right)$
$\mathrm{SU}(2)$ $\frac{1}{2}\sigma_c$	$\left(\frac{3}{4}\alpha - \frac{2}{g^4}\right) \sum_{P} \text{Tr}\left[P\right] - \frac{1}{2} \sum_{\mathbf{x},i,c} \left(F_{Q \mathbf{x},i}^c\right)^2$	$\alpha \sum_{\mathbf{x},i,c} \sum_{P \ni U_{\mathbf{x},i}} \vec{x}_P(U_{\mathbf{x},i}),$ $\vec{x}_P(U_1) = -\vec{x}_P(U_4) = \frac{1}{2} \operatorname{Tr} \left[\vec{\sigma} P \right]$ $\vec{x}_P(U_2) = \frac{1}{2} \mathcal{R}(U_1) \operatorname{Tr} \left[\vec{\sigma} P \right]$ $\vec{x}_P(U_3) = -\frac{1}{2} \mathcal{R}(U_4) \operatorname{Tr} \left[\vec{\sigma} P \right]$	$\sqrt{\Delta t}$	$g^2 \left(E_L + \frac{4}{g^2} N_{\text{plaquettes}} \right)$

TABLE II: Gauge group specific formulas for the implementation of a Green's Function Monte Carlo Solver. For U(1) the factor $s_P(U_{\mathbf{x},i})$ is equal to +1 when P contains $U_{\mathbf{x},i}$ and -1 when it contains $U_{\mathbf{x},i}^{\dagger}$. In the SU(2) formulas we use the rotation matrices $\mathcal{R}_b^a(U) = 2 \operatorname{Tr}[U\tau^a U^{\dagger}\tau^b]$.

Appendix A: Green's Function Monte Carlo for Hamiltonian Lattice Gauge Theories

To validate our simulations using digitised Hamiltonians, we compare to Hamiltonian simulations using Green's Function Monte Carlo Methods. Here one simulates the wave function $\psi(\mathbf{x})$ as an ensemble of random walkers $\{\ldots, \mathbf{x}_i, \ldots\}$ in configuration space. The density of walkers around a point \mathbf{x} then is understood as the value of $\psi(\mathbf{x})$. The ground state of a given system can then be found by performing a probabilistic imaginary time evolution. These methods have a rich history in nuclear physics [21, 22], but can also be applied to lattice gauge theories.

Our implementation is derived from references [20, 23, 24]. In particular, we aim to calculate the ground state energy and the ground state plaquette expectation value. Ref. [20] also suggests a method for estimating mass gaps. However, we did not yet reach satisfactory precision in our results. In the following we will give a quick overview of our implementation. For further details we recommend the cited references.

For lattice gauge theories it is common to not actually simulate the wave function itself, but the product of $\psi(\mathbf{x})\phi_{\text{Trial}}(\mathbf{x})$, where ϕ_{Trial} is typically a variational estimate of the ground state wave function. If chosen well, this can significantly reduce the variance of measured observables.

As a trial wave function we use

$$\phi_{\text{Trial}} = \frac{1}{N} \prod_{P} e^{\alpha \text{Tr}[\text{Re}(P)]}$$
 (A1)

where α is chosen such that $\langle \phi_{\text{Trial}} | \hat{H} | \phi_{\text{Trial}} \rangle$ is minimised. The algorithm itself can then be summarised by the following pseudo-code:

After initialising the ensemble of gauge configurations Ψ

Algorithm 1 Green's Function Monte Carlo. Input parameters of the algorithm for are the coupling g^2 , the step size Δt , the trial energy E_T , the number of sweeps

 $N_{\rm sweeps}$ and the number of propagation steps per branching step $N_{\rm hits}$. The gauge group specific formulas for $\tau_c, E_L, F_{Q\,\mathbf{x},i}^c$ and σ_χ can be found in tab. II

function GFMC(g^2 , Δt , E_T , $N_{\rm sweeps}$, $N_{\rm hits}$)

$$\begin{split} \Psi \leftarrow \left\{ C^1 = \{\dots, U^1_{\mathbf{x},i},\dots\},\dots, \\ C^{N_{\mathrm{target}}} = \{\dots, U^{N_{\mathrm{target}}}_{\mathbf{x},i},\dots\} \right\} \end{split}$$

▶ Random initial ensemble of gauge configurations

$$\vec{w} \leftarrow (1, \dots, 1)^T$$

$$\begin{array}{ll} \mathbf{for} \ s = 1, \dots, N_{\mathrm{sweeps}} \ \mathbf{do} \\ \mathbf{for} \ C_j \in \Psi \ \mathbf{do} \\ \mathbf{for} \ U_{\mathbf{x},i} \in C \ \mathbf{do} \end{array} \qquad \triangleright \text{Loop over configurations}$$

for
$$c = 1, ..., N_c$$
 do $\chi^c \leftarrow \text{random_normal}(\mu = 0, \sigma = \sigma_{\chi})$

$$\begin{array}{l} W_{\mathrm{rand}} \leftarrow \exp\left(-\sum_{c} \chi^{c} \tau_{c}\right) \\ \rhd \text{ Random component of the drift step} \end{array}$$

$$\begin{array}{c} W_{\text{force}} \leftarrow \exp\left(-\Delta t \sum_{c} F_{Q\,\mathbf{x},i}^{c}(C_{j})\tau_{c}\right) \\ \rhd \text{Force component of the drift step} \end{array}$$

$$\begin{aligned} U_{\mathbf{x},i} \leftarrow W_{\text{rand}} \cdot W_{\text{force}} \cdot U_{\mathbf{x},i} \\ & \triangleright \text{Apply the drift Step} \\ w_j \leftarrow w_j \exp\left(\Delta t (E_L - E_T)\right) \\ & \triangleright \text{Update the weights} \end{aligned}$$

if
$$s \mod N_{\text{hits}} = 0$$
 then \triangleright Branching Step

$$\Psi \leftarrow \Psi'$$
 s.t. w_j copies of C_j are in Ψ'

$$\vec{w} \leftarrow (1, \dots, 1)^T$$
 > Reset weights

and their respective weights \vec{w} , we enter the main loop of the algorithm. First is the drift step. Here the probabilistic imaginary time evolution is carried out. For this, each link is rotated by the sum of a quantum force term denoted as F_Q^c originating from the use of the trial wave function and a random number χ_c drawn from a normal distribution with variance σ_χ^2 . Next, the weight of each walker is adjusted according to the new energy of its configuration.

Lastly a branching step is performed every $N_{\rm hit}$ steps. Here a new ensemble Ψ' is created from the old ensemble Ψ by duplicating and deleting the random walkers in Ψ according to their weight. This ensures that the ensemble does not contain too many walkers with vanishing weights and thus implements a form of importance sampling. The fractional part in a given weight is treated probabilistically. E.g. a walker with a weight of $w_i=2.1$ has a 10% chance of appearing thrice in the new ensemble and a 90% chance of appearing twice.

The gauge group specific formulas for the energy E_L and the quantum force F_Q^c are summarised in table II, together with the other formulas needed in the implementation. As typically a renormalized Hamiltonian $\hat{H} \sim \hat{H}/g^2$ is simulated, the last column gives conversion formulas to obtain the spectrum of \hat{H} as given in section II from the configuration energy E_L .

1. Population Control

The branching step deserves a little more attention, as it introduces a problem. The trial energy E_T will need continuous tuning, as otherwise the population of random walkers will either grow or decay exponentially. Both cases are obviously not acceptable for practical applications.

Thus, some form of population control is needed. As discussed in [25], tuning E_T dynamically introduces a small bias to the results. For most method's this bias vanishes in the limit of infinitely large populations. As the sensitivity to E_T is quite high at weak couplings, a rather brute force version of population control was used. At the beginning of each branching step the weights are renormalized s.t.

$$\tilde{w}_i = \frac{N_{\text{target}}}{\sum_j w_j} w_j \,. \tag{A2}$$

Then N_{target} walkers were drawn from the old ones according to the renormalized weights \tilde{w}_i .

In our runs we use $N_{\rm target}=500\,000$. Thus, we expect the bias caused by population control to be quite small. As discussed earlier, good matching with other simulation methods is achieved up to 5 significant digits. However, it is likely that this bias needs to be investigated and addressed if one wants to achieve higher precision.

2. Observables

The ground state energy can be measured in two different ways. First one can take a weighted average of the configuration energies E_L after every sweep. This is the method we use will use in the following. Another option is to estimate the trial energy E_T , that keeps the size of the ensemble constant. Both should agree in the limit $\Delta t \to 0$.

To measure the plaquette expectation value we use the forward walking method as proposed in [20]. For this one first measures the average plaquette expectation value of each walker in a given ensemble. Then the ensemble is propagated like discussed before. However, during the branching steps we keep track of the ancestry of each walker. After a sufficient number of propagation steps we estimate the plaquette as the average of the plaquette expectation values of the initial ensemble, weighted by the weights of each configuration's descendants:

$$P = \frac{1}{\sum_{i} w_{\text{desc.}}^{i}} \sum_{i} w_{\text{desc.}}^{i} P_{\text{anc.}}^{i}$$
 (A3)

For a sufficient number of propagation steps this value eventually stabilises. An example of this can be seen in fig. 10a. To extract the stabilised value a function of the form

$$P(n) = P_{\infty} + b e^{-cn} \tag{A4}$$

is fitted to the data. P_{∞} is then taken as the estimator of the ground state plaquette expectation value.

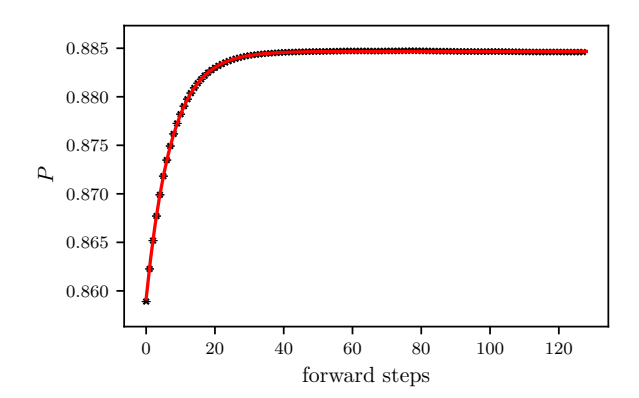
3. Statistics

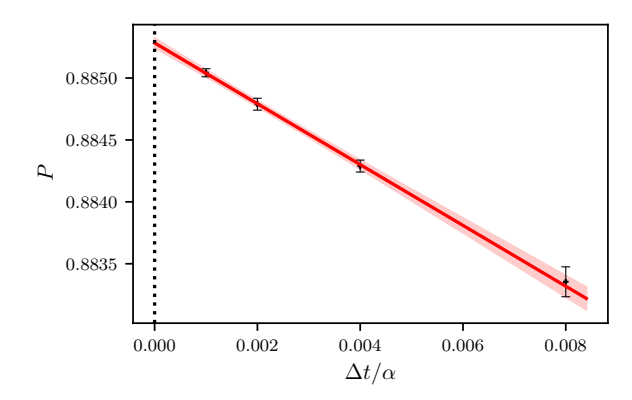
As stated earlier the ensemble size was chosen to be 500 000. Branching was performed every $N_{\rm hit}=5$ iterations. After a total $5\times 10\,000$ thermalisation iterations, initially at larger values of Δt , our measurement loop begins. It consists of 5×64 iterations to estimate the energy, followed by the forward walking plaquette measurement taken over 5×128 steps. P(n) is measured after each branching step in the forward propagation. These energy and plaquette measurements are then repeated a few hundred times. In total measurements are thus taken over more than $\mathcal{O}(5\times 20\,000)$ iterations.

For each cycle of the measurement loop the plaquette fit is carried out. The energies are estimated by taking the mean of E_L for the 5×64 initial sweeps. Errors are estimated by bootstrapping over all iterations of the measurement loop.

4. Extrapolating $\Delta t \to 0$

Lastly, each observable must be extrapolated to the limit $\Delta t \to 0$. As an example we show the plaquette expecta-





(a) The forward walking plaquette estimator as a function of the forward steps at $\Delta t = 0.002/\alpha$. Shown in red is the fit eq. (A4) used to estimate the plateau value.

(b) The ground state plaquette expectation value as a function of $\Delta t/\alpha$. In red, we show an extrapolation to $\Delta t \to 0$ which is used to estimate the physical value.

FIG. 10: Representative Extrapolations for the extraction of observables from the GFMC data. This particular set of plots is obtained from a 3^3 lattice with open boundary conditions at $g^2 = 0.2645$ using U(1) as a gauge group.

tion value as a function of $\Delta t/\alpha$ in fig. 10b. As can be seen, this is well described by a linear fit. The intersection with $\Delta t = 0$ finally gives us the values we used to compare to the digitised Hamiltonian results.

In our implementation we ran simulations at using four different time step sizes Δt given by

$$\Delta t \in \{0.008 \,\alpha, \, 0.004 \,\alpha, \, 0.002 \,\alpha, \, 0.001 \alpha\} \,.$$
 (A5)

Expressing Δt as a function of α proved useful, as it keeps the overall change by each drift step independent of the coupling.

5. Outlook

In general, the GFMC results proved quite useful in testing and benchmarking digitised Hamiltonian methods. We believe that it is worth reevaluating its potential capabilities considering the renewed interest in Hamiltonian lattice gauge theories as well as the advancements in computing power.